doi:10.1038/nature09129

LETTERS

Planar cell polarity breaks bilateral symmetry by controlling ciliary positioning

Hai Song[1], Jianxin Hu[1], Wen Chen[1], Gene Elliott[2], Philipp Andre[1], Bo Gao[1] & Yingzi Yang[1]

Defining the three body axes is a central event of vertebrate morphogenesis. Establishment of left–right (L–R) asymmetry in development follows the determination of dorsal–ventral and anterior–posterior (A–P) body axes[1,2], although the molecular mechanism underlying precise L–R symmetry breaking in reference to the other two axes is still poorly understood. Here, by removing both *Vangl1* and *Vangl2*, the two mouse homologues of a *Drosophila* core planar cell polarity (PCP) gene *Van Gogh* (*Vang*), we reveal a previously unrecognized function of PCP in the initial breaking of lateral symmetry. The leftward nodal flow across the posterior notochord (PNC) has been identified as the earliest event in the *de novo* formation of L–R asymmetry[3,4]. We show that PCP is essential in interpreting the A–P patterning information and linking it to L–R asymmetry. In the absence of *Vangl1* and *Vangl2*, cilia are positioned randomly around the centre of the PNC cells and nodal flow is turbulent, which results in disrupted L–R asymmetry. PCP in mouse, unlike what has been implicated in other vertebrate species, is not required for ciliogenesis, cilium motility, Sonic hedgehog (Shh) signalling or apical docking of basal bodies in ciliated tracheal epithelial cells. Our data suggest that PCP acts earlier than the unidirectional nodal flow during bilateral symmetry breaking in vertebrates and provide insight into the functional mechanism of PCP in organizing the vertebrate tissues in development.

Identifying the mechanism underlying the initial bilateral symmetry breaking has been an overriding goal in understanding how nature is able to produce organisms with consistent and distinct left and right anatomies. In mice, bilateral symmetry is broken by a leftward flow across a pit-like, teardrop-shaped PNC (also referred to as 'the node') generated by posteriorly localized motile cilia[3–6]. However, an earlier asymmetric event that positions the cilia to the posterior sides of PNC cells in response to the A–P patterning signals remains to be identified. PCP, which originally referred to an asymmetry of epithelial cells along an axis orthogonal to the apical–basal axis, is an evolutionarily conserved mechanism by which positional information is transmitted and maintained between and within cells[7]. A group of core PCP proteins including the transmembrane protein Vang have been identified in *Drosophila*[8]. Although mutants of core PCP genes have so far failed to show defects in L–R asymmetry, this is probably due to functional redundancy among members of a core PCP component. To overcome this and uncover important regulatory functions of PCP, we inactivated both *Vangl1* and *Vangl2*, the two mouse homologues of *Drosophila Vang*.

Vangl1 and *Vangl2* were broadly expressed during L–R patterning (Supplementary Fig. 1). Before the appearance of ciliated PNC cells, levels of Vangl1 and Vangl2 protein were too low to be detected. However, after embryonic day (E)7.75, the protein levels of both Vangl1 and Vangl2 were selectively and progressively upregulated in the PNC cells, and asymmetrical localization of Vangl1 and Vangl2 protein was observed along the A–P axis (Supplementary Fig. 2a–c), indicating that the PNC cells are indeed polarized and PCP may be required by the PNC cells to regulate early embryonic development. The Vangl1 and Vangl2 localization patterns are also consistent with the role of PCP in regulating convergent extension of neurulating vertebrate embryos[9]. In the sensory epithelia of the cochlea, Vangl1 and Vangl2 demonstrated similar asymmetrical localization patterns in both hair cells and supporting cells (Supplementary Fig. 2d, e). These data suggest that *Vangl1* and *Vangl2* are redundant in PCP, which should be severely disrupted by removing both *Vangl* genes.

A null allele of *Vangl1* (*Vangl1*^{gt}) was generated with a gene-trap embryonic stem-cell line (Supplementary Fig. 3). We also generated a floxed *Vangl2* allele, *Vangl2*^{f}, from which the null *Vangl2*$^{\Delta}$ allele was derived (Supplementary Fig. 3). *Vangl1* and *Vangl2* regulated PCP in a gene dose-dependent manner (Fig. 1 and Supplementary Fig. 4). Asymmetrical Vangl1 localization was still detected in the cochlea of the *Vangl2*$^{\Delta/\Delta}$ mutant (Fig. 1a). The *Vangl2*$^{\Delta/\Delta}$; *Vangl1*$^{gt/gt}$ embryos had the most severe developmental defects in comparison with embryos with other genotypes, particularly when sensory hair cell polarity and convergent extension were examined to assess PCP. Thus, *Vangl1* and *Vangl2* function of regulating PCP was removed in the *Vangl2*$^{\Delta/\Delta}$; *Vangl1*$^{gt/gt}$ embryos.

The *Vangl2*$^{\Delta/\Delta}$; *Vangl1*$^{gt/gt}$ embryos had multiple laterality defects, which were not detected in embryos with other genotypes (Fig. 2a). The *Vangl2*$^{\Delta/+}$; *Vangl1*$^{gt/+}$ mice were fertile, morphologically normal and served as controls in our study. The *Vangl2*$^{\Delta/+}$; *Vangl1*$^{gt/+}$ and *Vangl2*$^{\Delta/\Delta}$; *Vangl1*$^{gt/+}$ embryos always turned to the right side and their hearts correctly looped to the right ($n > 50$), but in all of the *Vangl2*$^{\Delta/\Delta}$; *Vangl1*$^{gt/gt}$ embryos assayed ($n > 10$), both embryonic turning and heart looping failed. In addition, the normal mouse lung has five lobes, four on the right and one on the left. In the *Vangl2*$^{\Delta/\Delta}$; *Vangl1*$^{gt/gt}$ embryos, however, mild left lung isomerism was observed with three lobes on the right side (4/9). Because PCP in visceral organs may also control morphogenesis in later stages, to assess the early L–R asymmetry defects in the *Vangl2*$^{\Delta/\Delta}$; *Vangl1*$^{gt/gt}$ embryos further, we examined the components in the Nodal signal cascade that are asymmetrically expressed and required for L–R patterning[10]. In control embryos, *Nodal* was first expressed symmetrically around the PNC (somite 0–1). Then, between somite 2 and somite 7 stages, *Nodal* expression on the left side of the PNC became progressively stronger and its expression in the left lateral plate mesoderm (LPM) was also detected[11,12]. In the *Vangl2*$^{\Delta/\Delta}$; *Vangl1*$^{gt/gt}$ embryos, however, *Nodal* expression around the PNC was decreased (6/11) (Fig. 2b, c). Strikingly, more robust *Nodal* expression on the right side of the PNC was also observed in the *Vangl2*$^{\Delta/\Delta}$; *Vangl1*$^{gt/gt}$ embryos (5/11) (Fig. 2b, c). In the LPM of *Vangl2*$^{\Delta/\Delta}$; *Vangl1*$^{gt/gt}$

[1]Developmental Genetics Section, Genetic Disease Research Branch, National Human Genome Research Institute, Bethesda, Maryland 20892, USA. [2]Transgenic Mouse Core, Genetic Disease Research Branch, National Human Genome Research Institute, Bethesda, Maryland 20892, USA.

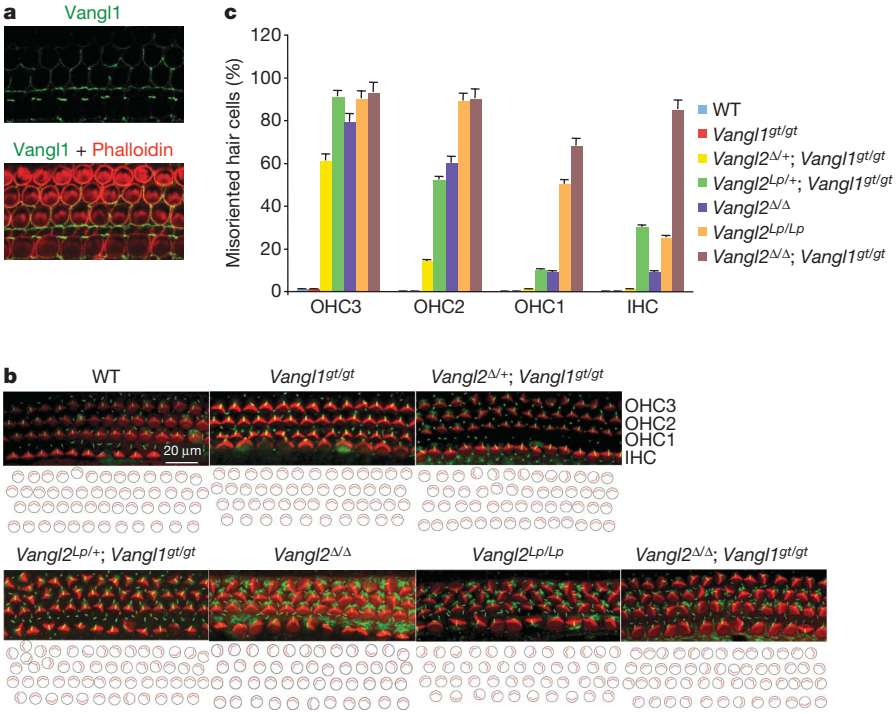

Figure 1 | The *Vangl2*$^{\Delta/\Delta}$; *Vangl1*$^{gt/gt}$ embryos have the most severe polarity defects. **a**, Asymmetrical localization of Vangl1 protein (green) in the sensory hair cells of the *Vangl2*$^{\Delta/\Delta}$ cochlea at E18.5. **b**, Sensory hair cell polarity at E18.5 is shown by the orientation of actin-based stereocilium bundles (red) and the microtubule-based kinocilia (green). WT, wild type. **c**, Quantification of misoriented hair cells in embryos with different genotypes. Results are means and s.d. for three samples. The orientation defects in the cochlea ranged from few misoriented cells (*Vangl2*$^{\Delta/+}$; *Vangl1*$^{gt/gt}$) to several affected cells (*Vangl2*$^{\Delta/\Delta}$, *Vangl2*$^{Lp/+}$; *Vangl1*$^{gt/gt}$ and *Vangl2*$^{Lp/Lp}$) to almost complete loss of polarity (*Vangl2*$^{\Delta/\Delta}$; *Vangl1*$^{gt/gt}$). OHC, outer hair cells; IHC, inner hair cells.

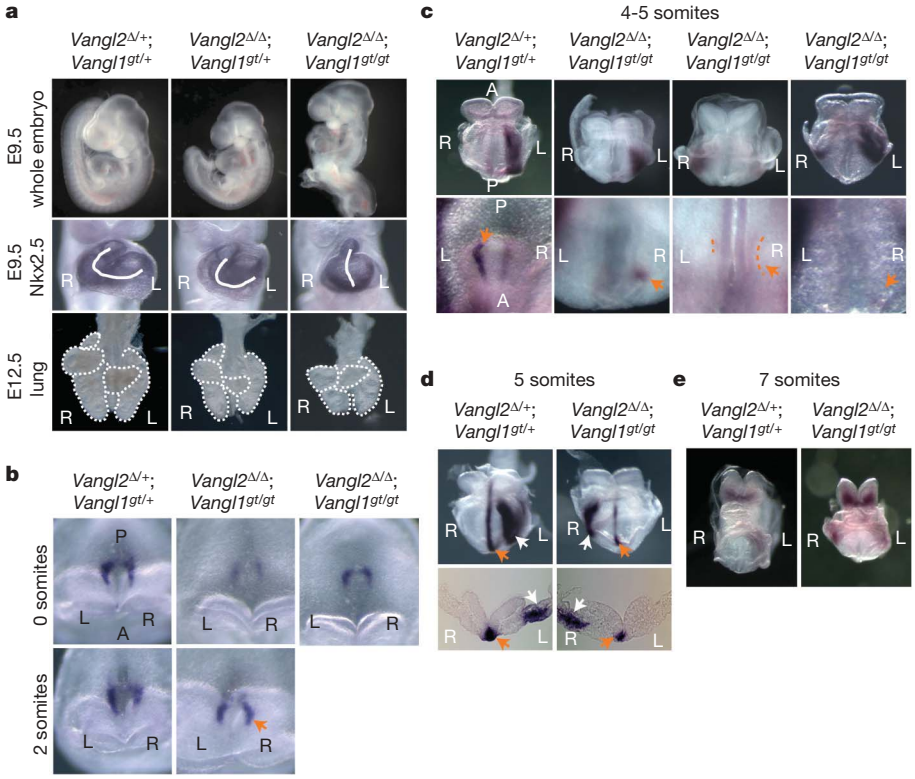

Figure 2 | Laterality defects in the *Vangl2*$^{\Delta/\Delta}$; *Vangl1*$^{gt/gt}$ embryos. **a**, Failure of embryonic turning and heart (marked by *Nkx2.5* expression) looping in the *Vangl2*$^{\Delta/\Delta}$; *Vangl1*$^{gt/gt}$ embryos. The *Vangl2*$^{\Delta/\Delta}$; *Vangl1*$^{gt/gt}$ lung has three lobes (outlined) instead of four on the right side. **b**, Perinodal *Nodal* expression is enhanced on the right side of the *Vangl2*$^{\Delta/\Delta}$; *Vangl1*$^{gt/gt}$ embryo (arrow). **c**, Ventral views of *Nodal* expression in LPM (top) and around the node (bottom, arrows). Weak perinodal *Nodal* expression is outlined. **d**, *Lefty1* expression (orange arrow) on the left side of prospective floor plate and *Lefty2* expression (white arrow) in the LPM, shown in ventral views (top) and transverse sections (bottom). **e**, Ventral views of *Pitx2* expression.

embryos, reversed (1/8) or bilateral (3/8) *Nodal* expression sites were observed (Fig. 2c). Controlled by Nodal signalling, expression of *Lefty1*, *Lefty2* and *Pitx2* was observed only on the left side of the control embryos[10,13–15]. In the double mutant embryos, *Lefty1* and *Lefty2* expression sites (1/2) were reversed (Fig. 2d) and bilateral *Pitx2* expression (2/7) was found (Fig. 2e). These results demonstrate that PCP is required upstream of *Nodal* to pattern the L–R axis. The incomplete penetrance of the laterality defects in the *Vangl1/2* mutant embryo is possibly due to one or more other inputs to the PCP pathway[16].

Because PCP has been implicated in ciliogenesis[17], we examined the morphology and movement of cilia in PNC cells. Cilia are long, thin microtubule-based projections from the basal bodies of most mammalian cells[18]. The PNC cell has a single motile cilium[3], which is essential for establishing leftward fluid flow across the ventral surface of the PNC. When examined by scanning electron microscopy and immunofluorescent labelling, cilia appeared normal in the PNC of the *Vangl2*$^{\Delta/\Delta}$; *Vangl1*$^{gt/gt}$ embryos ($n = 4$ in each case) at E8.0 (Fig. 3a, b). Thus, the L–R asymmetry defects in the *Vangl2*$^{\Delta/\Delta}$; *Vangl1*$^{gt/gt}$ embryos are not secondary to defects in ciliogenesis. The leftward nodal flow is enabled by the chirality of the cilium, as it rotates clockwise[3], and the posterior ciliary localization in the PNC cell, which results in a posterior tilt of the cilium and its rotation axis[5,6]. Because it has been postulated that the posterior positioning of the basal body might be controlled by PCP[6], we examined basal body localization in the PNC cells of the *Vangl* mutant embryos (Fig. 3c, d). The basal bodies were mostly localized posteriorly in both *Vangl2*$^{\Delta/+}$; *Vangl1*$^{gt/+}$ and *Vangl2*$^{\Delta/\Delta}$; *Vangl1*$^{gt/+}$ embryos. However, in the *Vangl2*$^{\Delta/\Delta}$; *Vangl1*$^{gt/gt}$ embryos the PNC cell density was slightly decreased (Supplementary Fig. 5a) and the number of posteriorly localized basal bodies was significantly decreased. Most basal bodies remained around the centre and anteriorly localized basal bodies were increased, resulting in an even distribution of basal bodies on the anterior and posterior sides of the PNC cells in the *Vangl2*$^{\Delta/\Delta}$; *Vangl1*$^{gt/gt}$ embryos (Fig. 3d and Supplementary Fig. 5b, c). This loss of posterior localization of basal bodies in the *Vangl* mutant was not a result of developmental delay (Supplementary Fig. 5c). Thus, posterior positioning of basal bodies in the PNC cells is indeed controlled by PCP, in the absence of which the basal bodies are mostly localized around the centre. Cilia in the PNC emerge from the centre of each cell at late streak stage (about E7.25). By early head fold stage (E7.75), most cilia are located in the posterior side of the PNC cells[6,19]. Because positioning of the kinocilium in sensory hair cells is also an event downstream of PCP[20], ciliary positioning may be a common readout of PCP.

To test whether altered ciliary positioning in the PNC cells affects function, we examined nodal flow (Fig. 4A and Supplementary Movies 1 and 2). In control embryos, fast and smooth leftward bead movement across the PNC was observed. In the *Vangl2*$^{\Delta/\Delta}$; *Vangl1*$^{gt/gt}$ embryos, bead movement was still biased leftwards, although beads were often trapped in swirling vortices and required more time to cross the PNC. Whereas the nodal flow of control embryos generated straight and parallel bead paths, in the mutant, bead paths contained 'knots' and abrupt turns and were often crossed with each other (2/2). When observed directly, the cilia in the PNC of the *Vangl2*$^{\Delta/\Delta}$; *Vangl1*$^{gt/gt}$ embryo were beating at a speed and direction similar to those of the control (Fig. 4B and Supplementary Movies 3 and 4). The abnormal nodal flow in the *Vangl2*$^{\Delta/\Delta}$; *Vangl1*$^{gt/gt}$ embryos also disrupted the left-biased perinodal rise of intracellular calcium in control embryos[21] (Fig. 4C, D). The incidence of bilateral increase or decrease in intracellular calcium concentration was increased in the *Vangl2*$^{\Delta/\Delta}$; *Vangl1*$^{gt/gt}$ embryos. The ectopic calcium signal on the right side was weaker and the domain was narrower and shorter. These results, taken together, show that unidirectionality of nodal flow was significantly

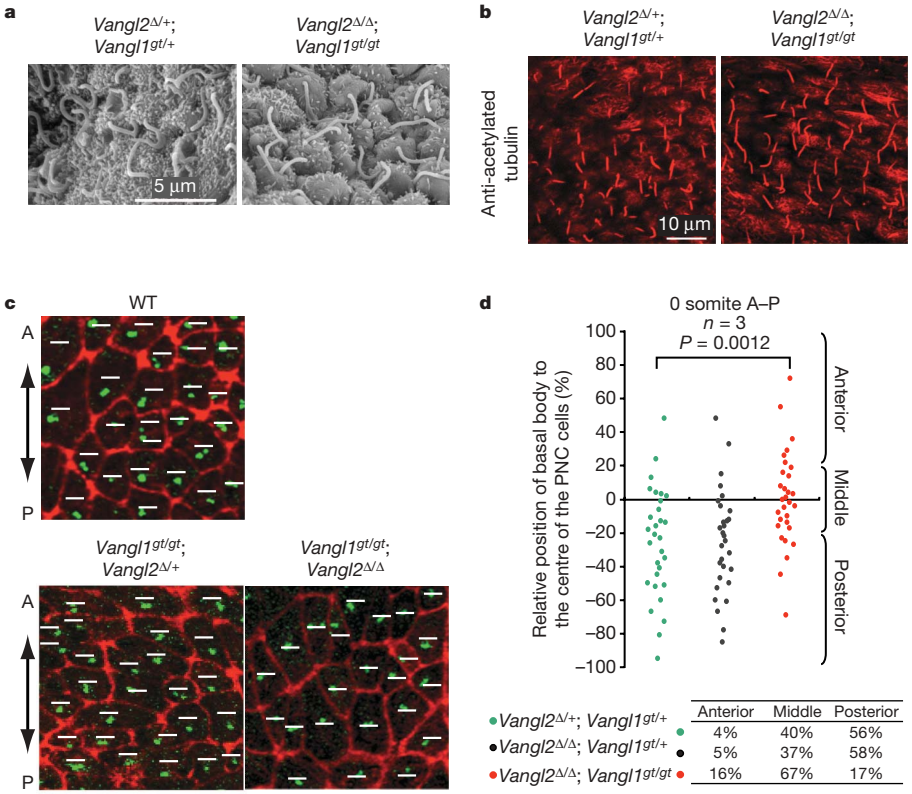

	Anterior	Middle	Posterior
Vangl2$^{\Delta/+}$; *Vangl1*$^{gt/+}$	4%	40%	56%
Vangl2$^{\Delta/\Delta}$; *Vangl1*$^{gt/+}$	5%	37%	58%
Vangl2$^{\Delta/\Delta}$; *Vangl1*$^{gt/gt}$	16%	67%	17%

Figure 3 | Randomized ciliary positioning in the *Vangl2*$^{\Delta/\Delta}$; *Vangl1*$^{gt/gt}$ embryos. **a**, Scanning electron microscopy of the PNC showing normal cilia at E8.0. **b**, Normal cilia (acetylated tubulin, red) in the PNC of the *Vangl2*$^{\Delta/\Delta}$; *Vangl1*$^{gt/gt}$ embryo at E8.0. **c**, Basal bodies (γ-tubulin, green) and cell boundaries (F-actin, red) of PNC cells at the 0-somite stage. White lines indicate the middle position along the A–P axis of each PNC cell. WT, wild type. **d**, Plot of relative positions of basal bodies to the midline (along the A–P axis) of the PNC cells. Posteriorly biased basal body positioning was lost in the *Vangl2*$^{\Delta/\Delta}$; *Vangl1*$^{gt/gt}$ embryos. The table shows percentages of PNC cells with indicated cilium localization.

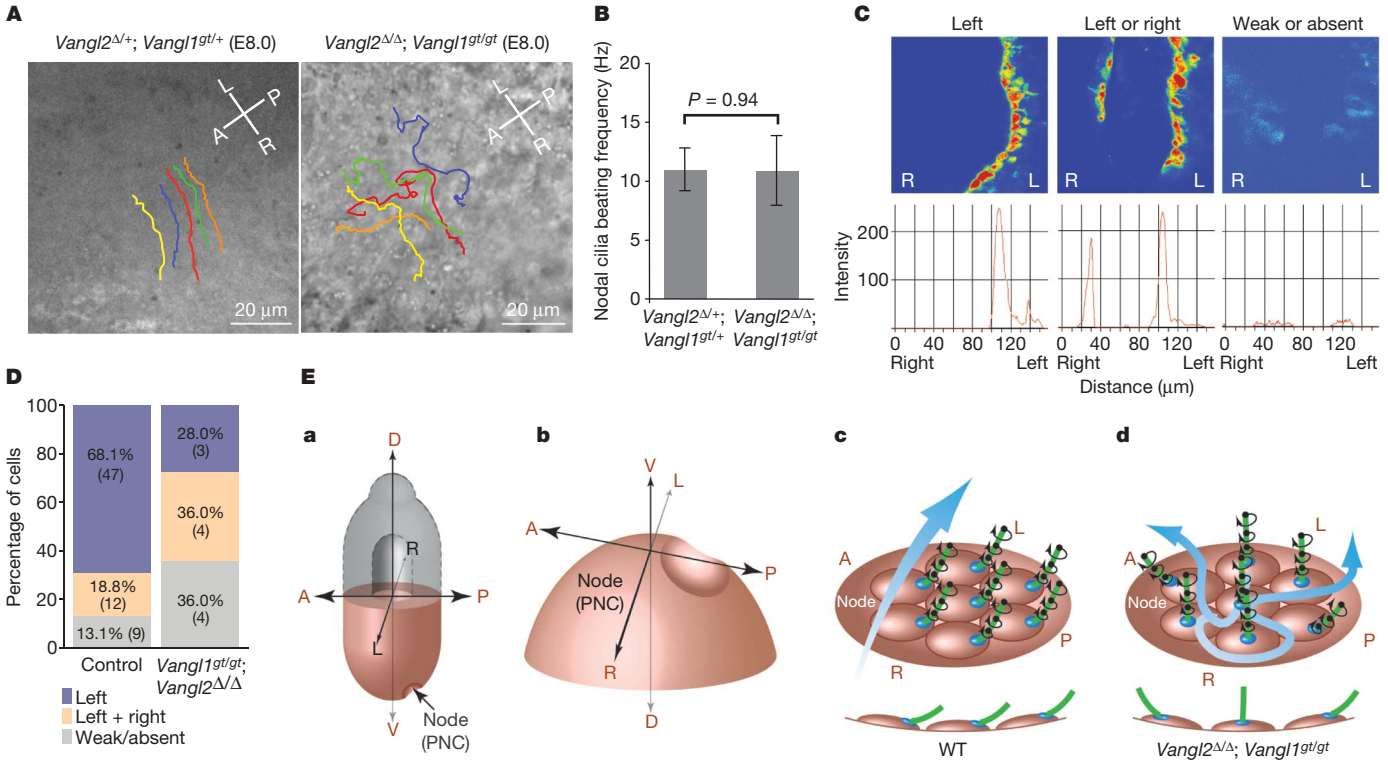

Figure 4 | *Vangl1* and *Vangl2* are required for normal leftward nodal flow. **A**, Nodal flow shown by tracing latex bead movement across the PNC with lines in different colours (Supplementary Movie 1, 2). **B**, Ciliary beating was recorded by live imaging (Supplementary Movies 3 and 4) and the mean beating frequency was calculated from at least ten nodal cilia of three embryos with indicated genotypes. Results are means ± s.d. **C**, Intracellular calcium release around the node, intensity scales are shown in the lower panels. **D**, Distribution of embryos (percentages and numbers) according to calcium patterns. **E**, Schematic diagram showing the role of *Vangl1* and *Vangl2* in breaking L–R symmetry. D, dorsal; V, ventral. **a**, A mouse embryo at E8.0. **b**, Enlarged distal view of **a**. **c**, Normal nodal flow generated by posteriorly positioned cilia. A side view of ciliated cells is shown in the lower panel. WT, wild type. **d**, In the $Vangl2^{\Delta/\Delta}$; $Vangl1^{gt/gt}$ embryo, randomly positioned cilia around the centre of the PNC cells resulted in aberrant, turbulent nodal flow.

compromised in the $Vangl2^{\Delta/\Delta}$; $Vangl1^{gt/gt}$ embryos. We have therefore identified PCP as the first step in breaking L–R symmetry by transmitting the A–P positional information to the PNC cells to enable posterior ciliary positioning (Fig. 4E).

Our data show that PCP is not required for ciliogenesis in the mouse (Fig. 1b and Supplementary Fig. 6c–f). In addition, Vangl1 and Vangl2 were not co-localized with cilia in any of the cells we examined, including the PNC cells, sensory hair cells, tracheal epithelial cells and floor plate cells (Supplementary Figs 2a, d and 6a, b). In the $Vangl2^{\Delta/\Delta}$; $Vangl1^{gt/gt}$ embryos at E18.5, there were no defects in ciliogenesis or docking of the basal bodies along the apical–basal axis of the multiciliate tracheal epithelial cells (Supplementary Fig. 6c, d). Normal Hedgehog signalling in the $Vangl2^{\Delta/\Delta}$; $Vangl1^{gt/gt}$ embryos and cells provides further evidence that primary cilia are functionally normal (Supplementary Figs 6g, h and 7).

To promote a robust break in symmetry, vertebrates have evolved mechanisms of early asymmetry initiation followed by asymmetry amplification and stabilization[22]. Because PCP is a major conserved molecular mechanism by which directional cellular and tissue behaviours are controlled through reorganizing the cytoskeleton, it could lead to both cilia-dependent and cilia-independent regulation of L–R asymmetry by controlling asymmetrical ciliary localization in ciliated PNC or cell movement around the node in the chick, which lacks ciliated PNC[5,6,23]. Involvement of PCP in regulating L–R asymmetry has been implicated previously: mutations in *Inversin* (*Inv*), *Bicaudal C* and *Seahorse* lead to L–R asymmetry defects upstream of *Nodal* expression, and these genes can interact with a core PCP gene, *Dishevelled* (*Dvl*)[24–26]. *Dvl* has recently been found to regulate ciliary localization in the PNC and has been implicated in the regulation of L–R patterning[27]. However, it is unlikely that *Inv* acts mainly through PCP because Inv, but not Vangl1/2, is localized to PNC cilia, and because the phenotypes of the *Inv* and *Vangl1/2* mutants are different in many aspects. Because abnormal L–R patterning is also associated with multiple congenital diseases[28], the availability of *Vangl1* and *Vangl2* conditional double mutants has opened a door to the investigation of the roles of PCP in many fundamental aspects of vertebrate development and diseases.

Note added in proof: While this work was in the press, two independent studies[29,30] were published; both also found that planar cell polarity mediated by *Vangl2* is required for orienting and positioning motile cilia.

METHODS SUMMARY

Scanning electron microscopic analysis. Embryos were dissected at E7.75 and fixed overnight in 2% glutaraldehyde, 4% paraformaldehyde, 0.1 M sodium cacodylate, pH 7.4 at 4 °C. Standard procedures were followed to prepare samples. Samples were examined with a Hitachi S-570 scanning electron microscope.

Analysis of calcium signalling. Embryos were dissected at E7.75–E8.0 and analysed in accordance with the established procedure[21].

Videomicroscopy. Embryos were dissected at E7.75–E8.0 in DMEM medium containing 20% FBS. The node was placed face down in a chamber with a coverslip on the bottom. Fluospheres (Invitrogen) were added into the medium to reveal the direction of nodal flow. Wide-field images were collected with a Personal DeltaVision system (Applied Precision Inc.) mounted on an inverted Olympus IX71 microscope with an oil-immersion Olympus Plan Apo N 60× 1.42 numerical aperture objective lens. Images were acquired with a CoolSNAP ES2 camera with 2 × 2 binning and an imaging field of 128 pixels × 128 pixels.

Full Methods and any associated references are available in the online version of the paper at www.nature.com/nature.

Received 25 January; accepted 26 April 2010.
Published online 20 June 2010.

1. Wilhelmi, H. Experimentelle Untersuchungen über situs inversus viscerum. *Arch. EntwMech.* **48**, 517–532 (1921).
2. Brown, N. A. & Wolpert, L. The development of handedness in left/right asymmetry. *Development* **109**, 1–9 (1990).

3. Nonaka, S. *et al.* Randomization of left–right asymmetry due to loss of nodal cilia generating leftward flow of extraembryonic fluid in mice lacking KIF3B motor protein. *Cell* **95,** 829–837 (1998).
4. Blum, M. *et al.* Ciliation and gene expression distinguish between node and posterior notochord in the mammalian embryo. *Differentiation* **75,** 133–146 (2007).
5. Nonaka, S. *et al.* De novo formation of left–right asymmetry by posterior tilt of nodal cilia. *PLoS Biol.* **3,** e268 (2005).
6. Okada, Y., Takeda, S., Tanaka, Y., Belmonte, J. C. & Hirokawa, N. Mechanism of nodal flow: a conserved symmetry breaking event in left–right axis determination. *Cell* **121,** 633–644 (2005).
7. Seifert, J. R. & Mlodzik, M. Frizzled/PCP signalling: a conserved mechanism regulating cell polarity and directed motility. *Nature Rev. Genet.* **8,** 126–138 (2007).
8. Axelrod, J. D. & McNeill, H. Coupling planar cell polarity signaling to morphogenesis. *ScientificWorldJournal* **2,** 434–454 (2002).
9. Jessen, J. R. *et al.* Zebrafish trilobite identifies new roles for Strabismus in gastrulation and neuronal movements. *Nature Cell Biol.* **4,** 610–615 (2002).
10. Hamada, H., Meno, C., Watanabe, D. & Saijoh, Y. Establishment of vertebrate left–right asymmetry. *Nature Rev. Genet.* **3,** 103–113 (2002).
11. Lowe, L. A. *et al.* Conserved left–right asymmetry of nodal expression and alterations in murine situs inversus. *Nature* **381,** 158–161 (1996).
12. Collignon, J., Varlet, I. & Robertson, E. J. Relationship between asymmetric nodal expression and the direction of embryonic turning. *Nature* **381,** 155–158 (1996).
13. Nakamura, T. *et al.* Generation of robust left–right asymmetry in the mouse embryo requires a self-enhancement and lateral-inhibition system. *Dev. Cell* **11,** 495–504 (2006).
14. Meno, C. *et al. lefty-1* is required for left–right determination as a regulator of *lefty-2* and *nodal*. *Cell* **94,** 287–297 (1998).
15. Yoshioka, H. *et al. Pitx2,* a bicoid-type homeobox gene, is involved in a Lefty-signaling pathway in determination of left-right asymmetry. *Cell* **94,** 299–305 (1998).
16. Lawrence, P. A., Struhl, G. & Casal, J. Planar cell polarity: one or two pathways? *Nature Rev. Genet.* **8,** 555–563 (2007).
17. Park, T. J., Haigo, S. L. & Wallingford, J. B. Ciliogenesis defects in embryos lacking inturned or fuzzy function are associated with failure of planar cell polarity and Hedgehog signaling. *Nature Genet.* **38,** 303–311 (2006).
18. Poole, C. A., Flint, M. H. & Beaumont, B. W. Analysis of the morphology and function of primary cilia in connective tissues: a cellular cybernetic probe? *Cell Motil.* **5,** 175–193 (1985).
19. Lee, J. D. & Anderson, K. V. Morphogenesis of the node and notochord: the cellular basis for the establishment and maintenance of left–right asymmetry in the mouse. *Dev. Dyn.* **237,** 3464–3476 (2008).
20. Jones, C. *et al.* Ciliary proteins link basal body polarization to planar cell polarity regulation. *Nature Genet.* **40,** 69–77 (2008).
21. McGrath, J., Somlo, S., Makova, S., Tian, X. & Brueckner, M. Two populations of node monocilia initiate left–right asymmetry in the mouse. *Cell* **114,** 61–73 (2003).
22. Tabin, C. J. The key to left–right asymmetry. *Cell* **127,** 27–32 (2006).
23. Gros, J., Feistel, K., Viebahn, C., Blum, M. & Tabin, C. J. Cell movements at Hensen's node establish left/right asymmetric gene expression in the chick. *Science* **324,** 941–944 (2009).
24. Kishimoto, N., Cao, Y., Park, A. & Sun, Z. Cystic kidney gene seahorse regulates cilia-mediated processes and Wnt pathways. *Dev. Cell* **14,** 954–961 (2008).
25. Maisonneuve, C. *et al.* Bicaudal C, a novel regulator of Dvl signaling abutting RNA-processing bodies, controls cilia orientation and leftward flow. *Development* **136,** 3019–3030 (2009).
26. Simons, M. *et al.* Inversin, the gene product mutated in nephronophthisis type II, functions as a molecular switch between Wnt signaling pathways. *Nature Genet.* **37,** 537–543 (2005).
27. Hashimoto, M. *et al.* Planar polarization of node cells determines the rotational axis of node cilia. *Nature Cell Biol.* **12,** 170–176 (2010).
28. Sharma, N., Berbari, N. F. & Yoder, B. K. Ciliary dysfunction in developmental abnormalities and diseases. *Curr. Top. Dev. Biol.* **85,** 371–427 (2008).
29. Guirao, B. *et al.* Coupling between hydrodynamic forces and planar cell polarity orients mammalian motile cilia. *Nature Cell Biol.* **12,** 341–350 (2010).
30. Borovina, A., Superina, S., Voskas, D. & Ciruna, B. Vangl2 directs the posterior tilting and asymmetric localization of motile primary cilia. *Nature Cell Biol.* **12,** 407–412 (2010).

Supplementary Information is linked to the online version of the paper at www.nature.com/nature.

Acknowledgements We thank members of the Yang laboratory for stimulating discussion; M. Kuehn, A. Kumar and J. Regard for critical reading of the manuscript; J. Fekecs and D. Leja for preparing the graphics; D. Wu for teaching us to dissect the mouse cochlea; and M. Kelley for the anti-Vangl2 antibodies. This study is supported by the intramural research programme of National Human Genome Research Institute.

Author Contributions H.S. designed and performed the experiments, generated most of the data in the manuscript, and interpreted and presented the data in figures. J.H. designed and performed some of the experiments, conducted statistical analysis, interpreted the data and put it together in figures. W.C. analysed and maintained the *Vangl1* mutant mice. G.E. generated the *Vangl1* and *Vangl2* mutant mice by performing blastocyst injection and tetraploid aggregation. P.A. and B.G. provided some critical technical support and help in writing the manuscript. Y.Y. designed and supervised the entire project, interpreted all data and wrote the manuscript.

Author Information Reprints and permissions information is available at www.nature.com/reprints. The authors declare no competing financial interests. Readers are welcome to comment on the online version of this article at www.nature.com/nature. Correspondence and requests for materials should be addressed to Y.Y. (yingzi@mail.nih.gov).

METHODS

Generation of and genotyping mouse lines. Generation of the floxed *Vangl2* allele is described in Supplementary Fig. 1e. *Vangl2*$^{\Delta}$ was generated by deleting exons 4 and 5 using the *Sox2–Cre* line[31]. *Vangl1*^{gt} allele was generated by using a Baygenomic gene-trap embryonic stem-cell line (XL802) (Supplementary Fig. 1a). Genotyping was performed with PCR using genomic DNA prepared from yolk sac or tail. Vangl2P1 (5′-CCATCGATGCACATGTGGTATC-3′) and Vangl2P2 (5′-GACAC TGTCCTCCATGTCCTTG-3′) were used to genotype the *Vangl2*^{f} allele and *Vangl2*$^{+}$ allele. Vangl2P1 and Vangl2P3 (5′-GCTATGACCAGCTACCTGAAG TC-3′) were used to genotype the *Vangl2*$^{\Delta}$ allele. Vangl1P1 (5′-CCCTGGC TTTCTTGTTGGTC-3′) and Vangl1P3 (5′-GGGCTGGCTCTTGGAGTCAT-3′) were used to genotype the *Vangl1*$^{+}$ allele. Vangl1P1 and Vangl1P2 (5′-CCTGGG GTTCGTGTCCTACA-3′) were used to genotype the *Vangl1*^{gt} allele.

Whole-mount *in situ* hybridization and LacZ staining. Whole-mount *in situ* hybridization and LacZ staining were performed as described previously[32]. Embryos were cryosectioned at 20 μm.

Immunofluorescence and antibodies. Embryos were fixed in 4% paraformaldehyde for 30 min at 4 °C, washed in PBS and incubated overnight in PBS containing 30% sucrose. Embryos were embedded in OCT compound (Tissue-Tek) and sectioned at 14 μm. Sections were permeabilized with 0.5% Triton X-100 in PBS and blocked for 1 h in 3% BSA, 0.1% Triton X-100 in PBS. Sections were incubated overnight with primary antibodies at 4 °C. Secondary antibodies were applied for 1 h at room temperature (22–25 °C). Primary antibodies used in immunofluorescence included mouse anti-Pax6, Pax7, Nkx2.2, Lim1/2, Nkx6.1, Hnf3β and Islet-1 (1:50 dilution; Developmental Studies Hybridoma Bank), rabbit anti-Olig2 (1:100; Abcam), mouse anti-acetylated-tubulin (1:5,000; Sigma), goat anti-γ-tubulin (1:200; Santa Cruz), goat anti-Vangl2 (1:100; Santa Cruz), rabbit anti-Vangl2 (1:50; gift from M. Kelley's laboratory) and goat anti-E-Cadherin (1:500; R&D). Vangl1 antibodies were generated against Vangl1 (residues 1–110) polypeptides fused to glutathione *S*-transferase in rabbit. Anti-Vangl1 antibodies were purified with the immunizing peptide coupled to Affigel (Bio-Rad). Alexa Fluor 488 and 568 of donkey anti-mouse, rabbit and goat secondary antibodies were from Invitrogen. Confocal images were acquired with a Zeiss LSM 510 NLO microscope. Excitation wavelengths of 488, 561 and 740 nm were used for the detection of secondary antibodies conjugated to Alexa Fluor 488, 568 and 4,6-diamidino-2-phenylindole, respectively.

Whole-mount immunostaining of cochlea or early E6–E8.5 embryos. Dissected cochlea or embryos were fixed for 30 min in 4% paraformaldehyde at 4 °C. Cochleae or embryos were permeabilized for 5 min with 0.5% Triton X-100 in PBS and blocked for 1 h in PBS with 3% BSA, 0.1% Triton X-100 at room temperature, followed by incubation overnight with primary antibodies at 4 °C. Cochleae or embryos were washed for 1 h in PBS with 0.1% Triton X-100 at room temperature, followed by incubation for 1 h with fluorescent secondary antibodies and Alexa Fluor-594-conjugated phalloidin (1:200; Invitrogen) at room temperature. The actin-based stereocilium bundles were shown by phalloidin staining, whereas the microtubule-based kinocilia or PNC cilia were shown by staining with the mouse anti-acetylated-tubulin antibody (1:5,000; Sigma). After being washed for 1 h with 0.1% Triton X-100 in PBS at room temperature, cochleae or the PNC region were flat mounted. Confocal images were acquired with a Zeiss LSM510 confocal microscope.

Immunoblot analysis. Embryonic tissues or cells were lysed in RIPA buffer. Cell lysates were analysed by immunoblotting. Primary antibodies used included goat anti-Vangl2 (1:2,000), rabbit anti-Vangl1 (1:1,000) and rabbit anti-Gli3 (1:5,000; gift from S. Mackem).

Analysis of calcium signalling. Embryos were dissected at E7.75–E8.0 and incubated for 20 min with the fluorescent calcium indicator Fluo-4 (Invitrogen) at 10 μM in DMEM with 20% FBS at 37 °C. Embryos were then washed three times in DMEM with 20% FBS and placed with the node facing upwards in a silicon chamber under a coverslip. Embryos were incubated for 20 min at 37 °C before confocal imaging. Confocal images were acquired with a Zeiss LSM510 confocal microscope. An excitation wavelength of 488 nm was used to detect Fluo-4. Embryos were genotyped after imaging. Data were analysed with Image-Pro 6.3 software. High intensity was shown in red and low intensity in blue. Intensity scales of the calcium signal were plotted from the left to the right side of the node.

Videomicroscopy. Embryos were dissected at E7.75–E8.0 in DMEM with 20% FBS. The node was placed facing downwards in a chamber with a coverslip bottom. For the nodal flow assay, Fluospheres (Invitrogen) were added into the medium to reveal the direction of nodal flow. Embryos were genotyped after imaging. Wide-field images were collected with a Personal DeltaVision system (Applied Precision Inc.) mounted on an inverted Olympus IX71 microscope with an Olympus Plan Apo N 60× 1.42 numerical aperture objective lens. All images were acquired with a CoolSNAP ES2 camera with 2 × 2 binning and an imaging field of 128 pixels × 128 pixels. Videos were created with SoftWoRx software package version 4.0.0 (Applied Precision). Individual bead movement was traced and shown as a line with a different colour. The mean cilia beating frequency was calculated from at least ten nodal cilia of embryos with indicated genotypes at E8.0. Results are means ± s.d. *P* was calculated with Student's *t*-test.

31. Hayashi, S., Tenzen, T. & McMahon, A. P. Maternal inheritance of Cre activity in a Sox2Cre deleter strain. *Genesis* **37**, 51–53 (2003).
32. Topol, L. *et al.* Wnt-5a inhibits the canonical Wnt pathway by promoting GSK-3-independent β-catenin degradation. *J. Cell Biol.* **162**, 899–908 (2003).